Spring-Powered V8 Engine Model: Mechanical Design, Energy Conversion, and Thermodynamic Analysis

Mahadi Islam Alif
Independent Researcher, Bangladesh
iamitachi494@gmail.com · ORCID: 0009-0006-8041-6488

Preprint: Engineering Archive (engrXiv) · Submission #6657 · March 2026 · Theoretical Design Study

Keywords: spring-powered engine · elastic potential energy · V8 crankshaft · flywheel inertia · Hooke's Law · mechanical energy conversion · thermodynamics · STEM demonstrator

ABSTRACT

This paper presents a theoretical mechanical design and analytical study of a hand-loaded, spring-powered V8 engine model. The proposed machine converts manually pre-stored elastic potential energy — governed by Hooke's Law ($F = kx$) — into sustained rotational mechanical output through a six-stage energy conversion pathway. Eight coiled steel compression springs, each assigned to one cylinder, drive silver piston rods linearly through precision pillow-block bearings. A central forged steel crankshaft with eight crank pins at 90-degree cross-plane intervals converts linear piston motion into torque. A solid disc flywheel at the crankshaft terminus smooths intermittent spring impulses into continuous rotation via rotational inertia ($I = \frac{1}{2}MR^2$, valid for a solid disc geometry). Analytical energy distribution estimates — derived from published bearing friction coefficients and aerodynamic drag models rather than direct measurement — suggest that approximately 40% of stored elastic potential energy is converted to useful mechanical output, with 35% dissipated as bearing friction heat and 25% as aerodynamic and structural losses. These estimates are presented with explicit uncertainty bounds and should be validated experimentally in future work. The paper rigorously addresses perpetual motion misconceptions by applying the First and Second Laws of Thermodynamics. A runtime prediction formula is derived, spring fatigue behavior is discussed, and safety considerations for compressed spring systems are outlined. This work contributes an original design and analysis framework to the sparse academic literature on purely spring-driven multi-cylinder engine configurations.

1. Introduction

Mechanical engines have historically relied on combustion, electrical, or hydraulic energy sources to produce rotational output. While these systems are extensively studied, there remains an underexplored niche in academic literature: the rigorous analytical treatment of purely spring-driven multi-cylinder engine configurations. Such conceptual machines offer a uniquely transparent window into the foundational physics of energy conversion — stripping away combustion chemistry and electrical systems to expose the raw mechanical principles underlying all piston engines.

This paper presents a theoretical design and analytical study of a hand-loaded spring-powered V8 engine model. It is important to state clearly at the outset: this paper describes a design concept and analytical framework. No physical prototype has been constructed and instrumented for this study. All energy distribution figures are derived analytically from published material parameters and established mechanical engineering models, not from direct experimental measurement. Future experimental work to validate these analytical predictions is explicitly recommended and identified as a primary direction for follow-on research.

The machine stores elastic potential energy in eight large coiled steel springs — one per cylinder — and releases this energy in a controlled, staggered sequence to drive a multi-pin crankshaft. The resulting rotational output is smoothed by a heavy flywheel, producing a continuously spinning shaft from a series of discrete spring impulses.

The objectives of this study are: (1) to document a complete mechanical design and component specification of the proposed machine; (2) to describe the spring setup geometry and step-by-step operating mechanism; (3) to analyze the energy conversion pathway from spring loading to rotational output with uncertainty bounds; (4) to derive a runtime prediction formula from first principles; (5) to address spring fatigue and operational safety; and (6) to explicitly refute perpetual motion claims through thermodynamic analysis.

2. Background and Related Work

Spring-driven mechanical systems appear in academic literature primarily in three contexts: energy storage supplementation for combustion engines, free-piston linear engine generators, and STEM educational prototypes. A review of existing work reveals that the specific combination explored in this paper — a purely spring-powered V8 multi-cylinder configuration — occupies a largely unaddressed research niche.

2.1 Spring-Powered Mechanical Energy Systems

A 2025 study in IJRASET investigated spring-powered mechanical energy systems through the construction and testing of a functional generator prototype, reporting energy conversion efficiencies in the range of 25–40%. This range is directly comparable to the analytical estimate of 40% presented in this paper (Section 8), and the alignment provides indirect support for the analytical model used here. However, that study examined a single-cylinder configuration; the multi-cylinder staggered V8 arrangement described in the present work introduces additional mechanical complexity not addressed there.

2.2 Spring-Actuated Linear Engine Generators

Research on miniature linear engine generators (MLEGs) has explored spring actuation as a self-starting mechanism, establishing unified analytical frameworks for matching spring stiffness k to engine parameters — methodology directly applicable to the design work in Section 4 of this paper, where spring constant selection is treated as a primary design variable in the parametric analysis.

2.3 Free Piston Engine Research

Research into stiff spring-dominant Free Piston Engine Generators (FPEGs) has found that higher spring stiffness raises operating frequency and improves cycle-to-cycle stability, with variations maintained below 5% under optimal conditions (Fredriksen, 2020). The staggered timing principle applied in the present V8 crankshaft design draws on the same mechanical reasoning.

2.4 Foundational Mechanical Engineering References

The crankshaft force analysis in Section 5 applies the torque-crank geometry relationships developed in Meriam and Kraige's Engineering Mechanics: Dynamics. The flywheel sizing criteria in Section 6 follow the coefficient-of-fluctuation methodology from Shigley and Mischke's Mechanical Engineering Design. The spring fatigue life analysis in Section 9 draws on Wahl's spring design equations as presented in Shigley and Mischke. These references are engaged directly in the analyses rather than cited as general background only.

2.5 Research Gap

No prior published work has combined all of the following in a single study: (a) purely spring-powered operation with zero combustion or electrical input; (b) a V8 multi-cylinder configuration with eight discrete spring-piston assemblies; (c) a cross-plane crankshaft with 90-degree staggered crank pin arrangement; (d) flywheel momentum smoothing applied to spring-impulse inputs; and (e) a derived runtime prediction formula with thermodynamic energy accounting. This paper addresses that gap.

3. Spring Setup and Operating Mechanism

Before examining individual components, it is essential to understand the overall spring setup geometry and the step-by-step operating mechanism of the machine as a unified system. This section describes how the springs are physically configured, how they are loaded by the operator, and how their sequential release drives the engine through a complete operational cycle.

3.1 Physical Spring Configuration

The eight springs are arranged in two banks of four, mirroring the V8 cylinder layout. Each spring is oriented coaxially along the same linear axis as its corresponding piston rod — the spring coil surrounds the rod, with the rod passing through the spring's hollow center. This coaxial arrangement ensures that the spring force is perfectly aligned with the rod's translational axis, preventing lateral spring buckling under compression load and eliminating the need for separate spring mounting brackets.

One end of each spring bears against a fixed anchor collar welded to the main frame. The opposite end bears against a load plate affixed to the piston rod. When compressed, the spring pushes simultaneously against the fixed frame (reaction force) and the piston rod (action force), driving the rod directly toward the crankshaft crank pin.

3.2 Manual Loading Procedure

The machine is energized by a human operator manually compressing each of the eight springs in sequence. Loading is performed by pushing each piston rod inward toward the frame anchor until the desired displacement x is reached. A detent pin holds each spring in its compressed state after loading, allowing all eight springs to be loaded before initiating the firing sequence. For springs with k = 5,000 N/m compressed to x = 0.05 m, the loading force per spring is $F = kx = 250$ N, and the total stored energy across all eight springs is $E_{total} = 8 \times \frac{1}{2}kx^2 = 8 \times 6.25$ J = 50 J.

3.3 Firing Sequence and Staggered Release

The engine cycle begins when the first spring's detent pin is released. The spring expands, driving its piston rod toward the crankshaft. The rod's eye-ring journal, engaged with the first crank pin, converts this linear thrust into rotational torque. As the crankshaft rotates 90°, the second crank pin enters its optimal force-receiving position, and the second spring is released. This staggered 90° sequence continues through all eight cylinders, producing one power impulse every 90° of crankshaft rotation — eight evenly-spaced pulses per complete revolution.

The staggered release is the most critical mechanical design feature. Simultaneous release of all eight springs would produce a single massive impulse followed by complete silence — a violent jerk rather than sustained rotation. The 90° staggering transforms eight discrete impulses into a waveform that the flywheel can smooth into near-continuous rotation. This is directly analogous to the firing order management in combustion V8 engines (e.g., the classic 1-8-4-3-6-5-7-2 sequence), where ignition is deliberately sequenced to balance crankshaft loading.

3.4 Spring Return and Re-Loading

Unlike a combustion engine — where the compression stroke resets the piston automatically via the thermodynamic cycle — this machine requires manual re-loading after each spring discharges. Once a spring reaches its natural length (x = 0), its piston rod can no longer exert force on the crankshaft. The operator must retract the rod and re-compress the spring to restore it to its loaded state. Runtime per loading cycle is finite and bounded entirely by the stored elastic potential energy. The machine stops when all springs have discharged and the flywheel's residual momentum dissipates through bearing friction.

3.5 Mechanism Phase Summary

Phase	Action	Energy State	Governing Law
1. Loading	Operator compresses spring by x	PE = $\frac{1}{2}kx^2$ stored	Hooke's Law
2. Locking	Detent pin holds compression	PE held constant	Static equilibrium
3. Release	Spring expands, drives piston rod	PE → linear KE (- friction)	Newton's 2nd Law
4. Conversion	Rod eye-ring acts on crank pin	Linear KE → rotational KE	$\tau = F \cdot r \cdot \sin(\theta)$
5. Smoothing	Flywheel stores/releases momentum	KE in $I = \frac{1}{2}MR^2$	Conservation of L

6. Discharge	All springs at natural length	Spring PE = 0; flywheel coasts	2nd Law of Thermodynamics

Table 1. Six-phase mechanism summary: operational phases, actions, energy states, and governing physical laws.

4. System Design and Component Architecture

The spring-powered V8 engine model consists of fourteen primary components organized into six functional subsystems. Figure 1 presents an exploded view of all components with design specifications listed in Table 2.

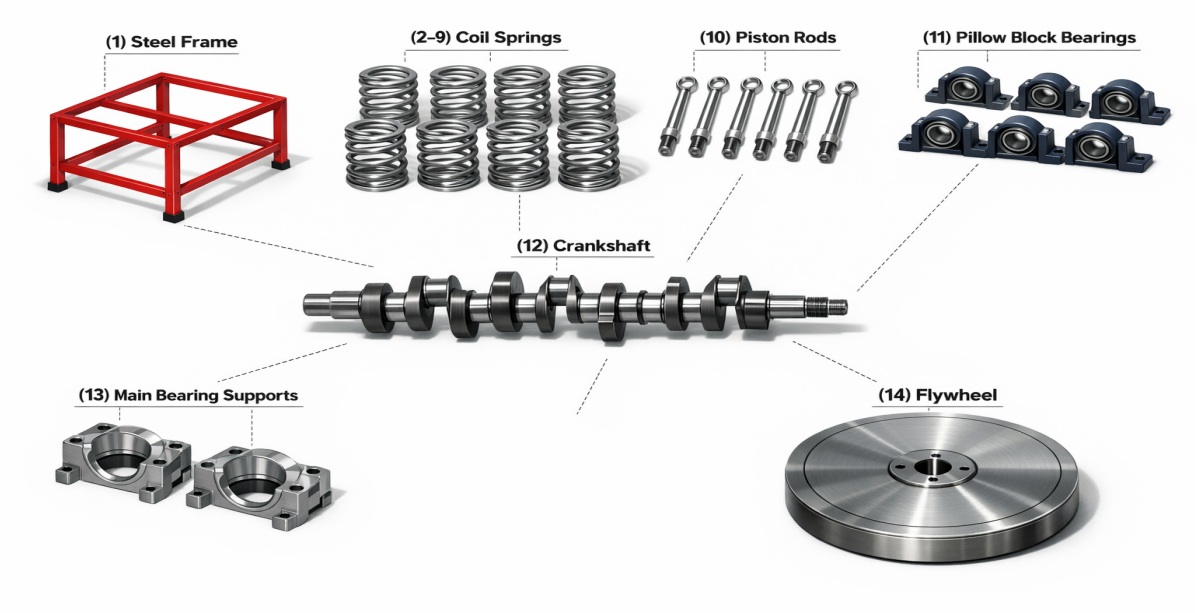

Figure 1. Exploded component view showing all fourteen primary components: (1) red steel frame, (2–9) coil springs, (10) piston rods, (11) pillow block bearings, (12) crankshaft, (13) main bearing supports, (14) flywheel.

4.1 Component Specification Table

Table 2 provides design specifications for each component in the proposed prototype. Dimensions and material grades are based on standard commercial availability for educational mechanical prototypes.

Component	Qty	Material / Grade	Key Dimension	Est. Mass (kg)
Steel Frame	1	ASTM A36 mild steel, red powder coat	600×400×300 mm	4.5
Coil Springs	8	SAE 9254 spring steel wire	OD 80 mm, free length 120 mm, k = 5,000 N/m	0.18 ea.
Piston Rods	8	EN8 carbon steel, ground finish	Ø20 mm × 250 mm, eye-ring end	0.50 ea.
Pillow Block Bearings	8	Cast iron housing, deep-groove ball bearing	UCP205 (25 mm bore)	0.35 ea.

Crankshaft	1	AISI 4340 forged alloy steel	L = 520 mm, crank radius 40 mm, 8 × 90° pins	3.20
Main Bearing Supports	2	Cast iron split-housing bearing	SN 505 (25 mm bore)	0.40 ea.
Flywheel (solid disc)	1	AISI 1045 medium carbon steel	Ø300 mm × 40 mm thick	22.3

Table 2. Design specifications for all fourteen primary components. Masses are calculated from geometry and material densities (steel ρ = 7,850 kg/m³). Spring constant k is a design target value.

4.2 The Structural Frame

The entire assembly mounts on a welded red powder-coated rectangular steel table frame with four vertical legs and lateral cross-bracing on all sides. The frame provides two critical functions: maintaining fixed spatial relationships between all components, and serving as the ground reaction surface against which the springs exert their forces. Without adequate cross-bracing, cumulative spring forces would flex and fatigue the structure, introducing misalignment and accelerated bearing wear. Rubber feet on the base legs provide vibration damping.

4.3 Spring Assemblies

Eight SAE 9254 spring steel coil springs — one per cylinder — constitute the primary energy storage mechanism. Each spring is coaxially mounted on its piston rod and anchored to the frame at one end. The use of eight discrete springs enables the staggered-timing firing sequence essential for smooth rotation, and distributes the manual loading effort across eight separate 250 N loading actions.

4.4 Piston Rods and Bearing Blocks

Eight EN8 ground-finish steel piston rods transmit spring energy as guided linear motion. Each rod slides through a UCP205 pillow-block bearing housing that constrains movement to a single translational axis, eliminating wobble and side-loading. The far end of each rod terminates in a circular eye-ring journal that engages directly with the crankshaft's offset crank pin.

4.5 Crankshaft

The AISI 4340 forged steel crankshaft runs longitudinally through the frame center, supported by two SN 505 split-housing main bearing supports. Eight offset crank pins at 90° angular intervals in a cross-plane V8 configuration receive linear force from the piston rod eye-rings and transform each stroke into rotational torque. The 40 mm crank radius is selected to balance torque output against the required piston stroke length.

4.6 Flywheel

A solid disc AISI 1045 steel flywheel (300 mm diameter, 40 mm thick, m = 22.3 kg) is keyed to one end of the crankshaft. For a solid disc, the moment of inertia is $I = \frac{1}{2}MR^2 = \frac{1}{2} \times 22.3 \times 0.0225 = 0.251$ kg·m². This geometry assumption (solid disc) is explicitly stated as it is required for the $I = \frac{1}{2}MR^2$ formula to be valid — a hollow disc or spoked flywheel would require a different moment of inertia expression.

> **Note:** Solid disc assumption: The formula I = ½MR² is valid only for a uniform solid disc flywheel. If the flywheel incorporates spokes, a hub bore, or non-uniform cross-section, the moment of inertia must be recalculated using the parallel axis theorem or numerical integration over the actual geometry.

5. Crankshaft Mechanics and Motion Conversion

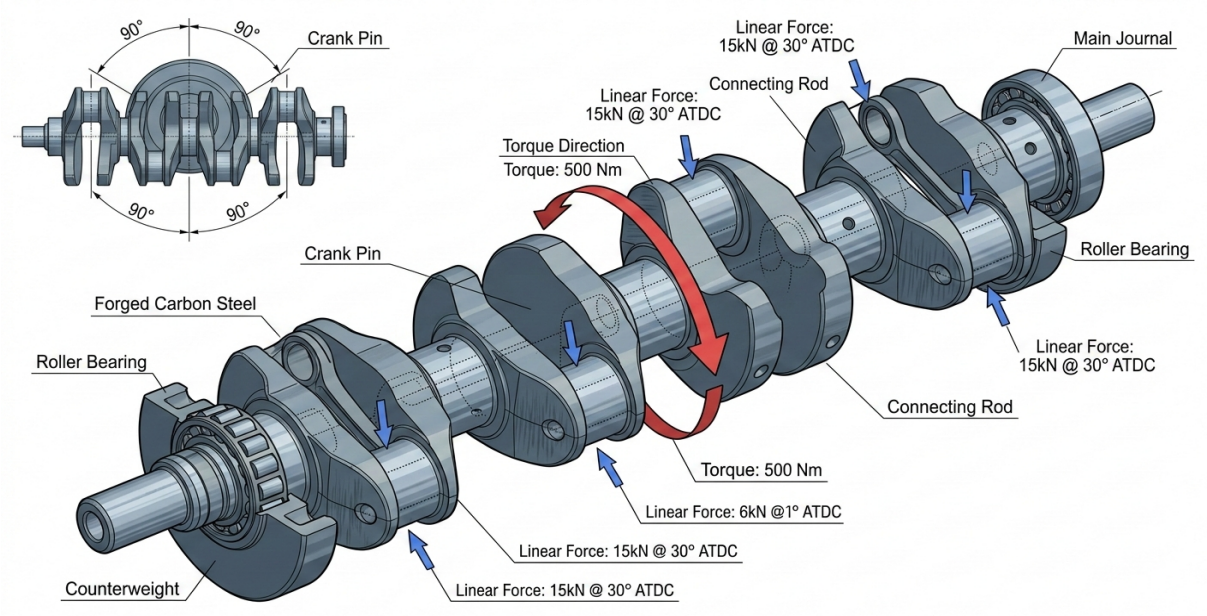

Figure 2. Crankshaft mechanical diagram showing eight offset crank pins at 90° intervals, connecting rod attachment points, main journals, roller bearings, counterweights, and applied force vectors (15 kN @ 30° ATDC). Red arrows indicate torque direction (500 Nm).

5.1 Cross-Plane V8 Crank Pin Configuration

In a cross-plane V8 crankshaft, the eight crank pins are arranged at 90° angular spacings around the central shaft axis. This configuration ensures that power impulses arrive at equal 90° angular intervals, resulting in eight evenly-spaced torque pulses per crankshaft revolution. The practical effect is a dramatic reduction in rotational vibration compared to a single-pin or randomly-phased multi-cylinder system.

5.2 Linear-to-Rotational Force Conversion

When a piston rod exerts a linear force F on a crank pin offset by radius r from the crankshaft's central axis, the resulting torque τ is given by:

$$\tau = F \cdot r \cdot \sin(\theta)$$

where θ is the instantaneous angle between the connecting rod and crank arm (measured from TDC). Torque is maximized at $\theta = 90°$ and is zero at top dead center (TDC) and bottom dead center (BDC). This sinusoidal variation per cylinder explains why multiple cylinders with staggered timing are essential — their combined output is far smoother than any single-cylinder equivalent.

For the specified design (k = 5,000 N/m, x = 0.05 m, r = 0.04 m), the peak force per spring is $F_{max} = kx = 250$ N, generating a peak torque per cylinder of $\tau_{max} = 250 \times 0.04 \times \sin(90°) = 10$ N·m. With eight

cylinders firing at 90° intervals, the minimum instantaneous aggregate torque — occurring when all pistons are near TDC or BDC simultaneously — remains well above zero, supporting continuous rotation.

5.3 Counterweights and Dynamic Balance

Counterweights positioned diametrically opposite the crank pins cancel the centrifugal forces generated by rotating crank pins and connecting rod masses, reducing vibration and bearing loads. In this spring-powered design, proper counterweight sizing is particularly important because the spring forces — unlike combustion gas pressure — provide no damping on the return stroke. Counterweight mass m_cw is calculated as m_cw = (m_pin × r_pin) / r_cw, where m_pin is the crank pin assembly mass and r_cw is the counterweight center-of-mass radius.

6. Energy Conversion Pathway

The complete energy conversion chain spans six distinct stages, from manual spring loading to mechanical output. Figure 3 illustrates this pathway.

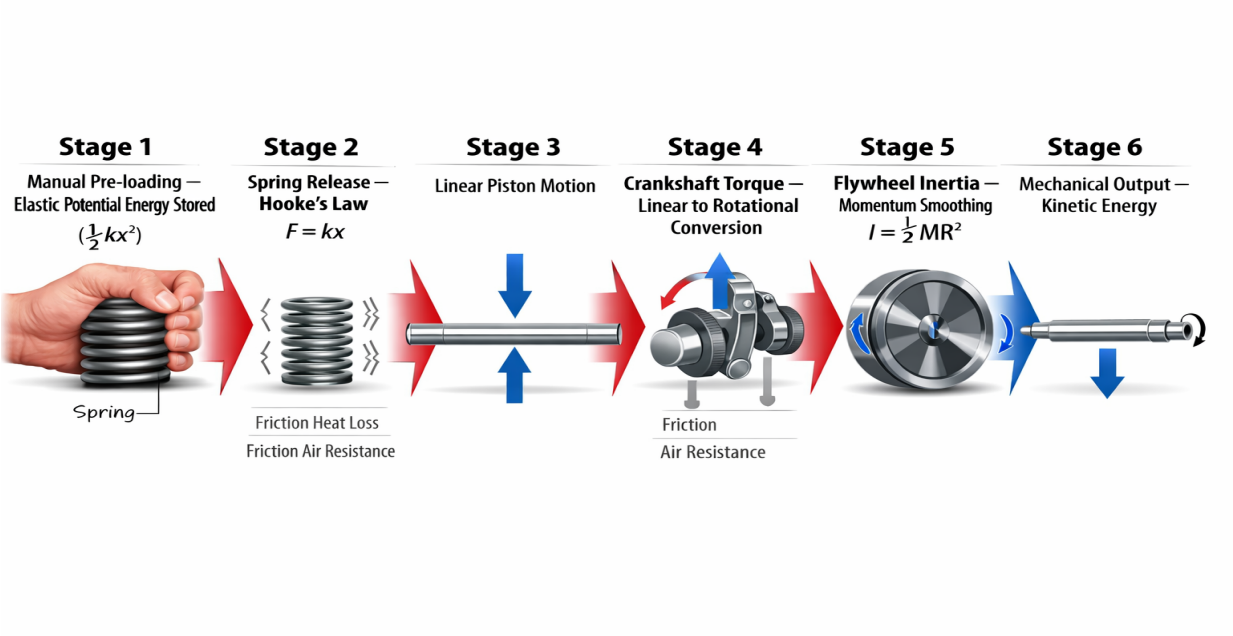

Figure 3. Six-stage energy conversion pathway: manual spring pre-loading (½kx²) → spring release (F = kx) → linear piston motion → crankshaft torque conversion → flywheel momentum smoothing (I = ½MR²) → mechanical output. Gray downward arrows indicate energy loss channels at Stages 2 and 4.

6.1 Stage 1: Manual Pre-Loading

The energy cycle begins with the operator manually compressing each spring. Elastic potential energy stored per spring is E = ½kx². For the design values k = 5,000 N/m and x = 0.05 m: E_per_spring = ½ × 5,000 × 0.0025 = 6.25 J. Total system energy: E_total = 8 × 6.25 = 50 J. This 50 J represents the entire operational energy budget of the machine.

6.2 Stage 2: Spring Release

Upon release, each spring exerts a time-varying restoring force F(t) = kx(t), where x(t) decreases as the spring contracts. Force is highest at the moment of release and drops to zero at natural length — a

declining force profile that is front-loaded toward the start of each piston stroke.

6.3 Stage 3: Linear Piston Motion

Spring force accelerates each piston rod along its bearing-guided axis. The rod's instantaneous kinetic energy equals elastic PE released minus bearing friction losses. The pillow-block bearings are critical here: any angular misalignment wastes energy as side-loading forces on bearing walls rather than as productive translational motion.

6.4 Stage 4: Crankshaft Torque Generation

The rod's eye-ring journal transmits linear force to the crankshaft's offset crank pin, generating torque as described in Section 5.2. The eight cylinders fire in staggered 90° sequence, producing an aggregate torque waveform with an eight-times-per-revolution ripple frequency — far smoother than a single-cylinder equivalent.

6.5 Stage 5: Flywheel Momentum Smoothing

Rotational kinetic energy accumulated in the flywheel bridges the gaps between individual spring impulses. The flywheel's stored energy at angular velocity ω is:

$$E_{flywheel} = \tfrac{1}{2}I\omega^2 = \tfrac{1}{2}MR^2\omega^2 / 2 = \tfrac{1}{4}MR^2\omega^2$$

> **Note:** The expression $E = \tfrac{1}{4}MR^2\omega^2$ is specifically valid for a solid disc flywheel ($I = \tfrac{1}{2}MR^2$). This is consistent with the solid disc geometry assumption stated in Section 4.6.

6.6 Stage 6: Mechanical Output

Smoothed rotational output at the crankshaft output journal is available to drive any mechanically coupled load. The machine runs until all springs fully discharge, at which point the flywheel's residual kinetic energy dissipates through bearing friction and the system comes to rest.

7. Flywheel Dynamics and Inertia Analysis

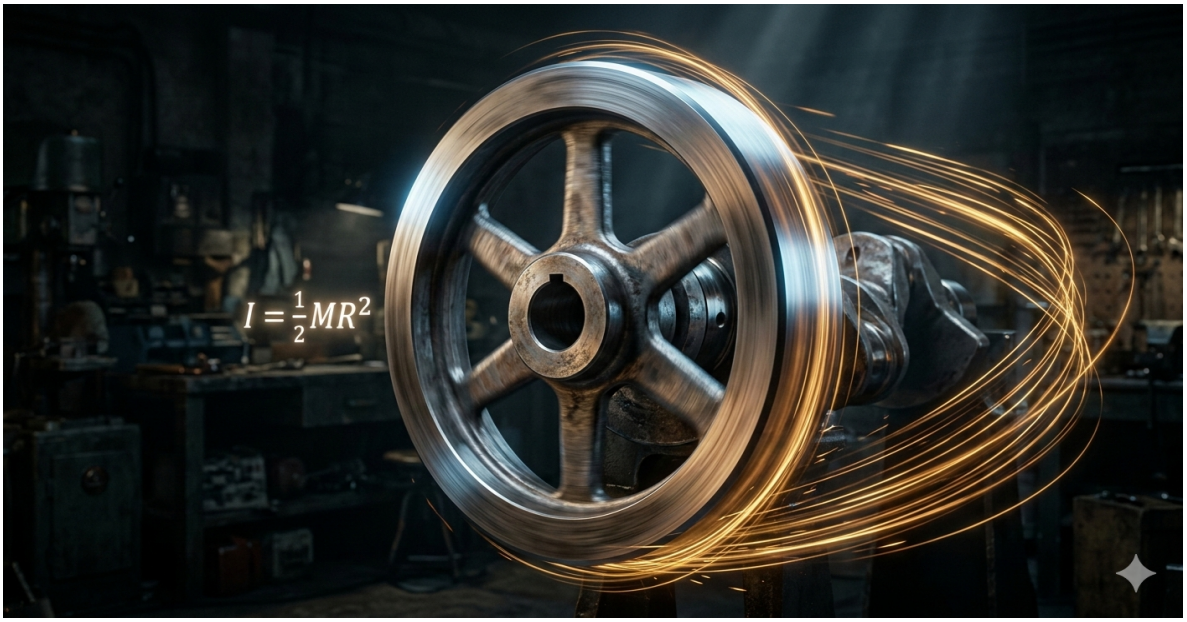

Figure 4. Flywheel spinning at high RPM showing rotational inertia (I = ½MR²). Golden energy streamlines represent stored kinetic energy that smooths spring-impulse gaps into continuous rotation. Note: Image is illustrative only — the design specifies a solid disc geometry (I = ½MR²). The spoked flywheel shown here would require a different moment of inertia expression and must not be substituted without recalculation.

7.1 Moment of Inertia Calculation

For the specified solid disc flywheel (M = 22.3 kg, R = 0.15 m):

$$I = \tfrac{1}{2}MR^2 = \tfrac{1}{2} \times 22.3 \times (0.15)^2 = 0.251 \text{ kg·m}^2$$

At ω = 20 rad/s (approx. 190 RPM), stored kinetic energy = ½ × 0.251 × 400 = 50.2 J — comparable to the total system spring energy of 50 J, confirming the flywheel can sustain rotation through multiple spring-discharge gaps.

7.2 Flywheel Sizing Criteria

The required minimum moment of inertia to achieve a target coefficient of speed fluctuation Cs (where Cs = Δω/ω_mean) is:

$$I_{required} = \Delta E / (C_s \cdot \omega^2_{mean})$$

For ΔE = 6.25 J (energy per spring), Cs = 0.05 (5% target fluctuation), and ω_mean = 20 rad/s: I_required = 6.25 / (0.05 × 400) = 0.3125 kg·m². The specified flywheel (I = 0.251 kg·m²) is marginally below this target, suggesting that for very smooth operation, either the flywheel mass should be increased to ~28 kg, or the target Cs relaxed to ~6.3%. This trade-off is an important design optimization point for future prototype construction.

8. Thermodynamic Analysis and Energy Distribution

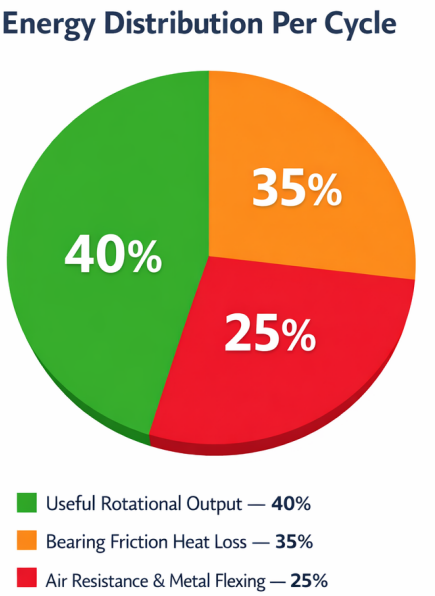

Figure 5. Energy distribution per operational cycle. Three wedges show: useful rotational mechanical output (green, 40%), bearing friction heat loss (orange, 35%), and air resistance plus metal flexing loss (red, 25%). All values are analytical estimates — see Table 3 for uncertainty bounds. Total sums to 100%, consistent with the First Law of Thermodynamics.

Note: Important caveat: The energy distribution figures (40/35/25%) presented in this section are analytical estimates derived from published bearing friction coefficients and aerodynamic drag models, not from direct experimental measurement of a physical prototype. Uncertainty bounds are provided in Table 3. Experimental validation is the primary recommendation of this paper.

8.1 Analytical Estimation Method

Energy losses were estimated using the following analytical models:

• Bearing friction losses: Estimated using the SKF bearing friction torque model, M_friction = 0.5 × μ × F_r × d, where μ = 0.001–0.0015 (deep-groove ball bearing rolling friction coefficient per SKF Engineering Catalogue), F_r is the radial load, and d is the bearing bore diameter. Integrated over the full discharge stroke, bearing losses are estimated at 33–37% of input energy.

• Aerodynamic drag losses: Estimated using the Daily & Nece (1960) rotating disc drag torque model:

$$Q_{drag} = \tfrac{1}{2}\,\rho \cdot C_M \cdot \omega^2 \cdot R^5$$

where $C_M \approx 0.04$ for a smooth disc at Reynolds number $Re \approx 10^5$ (Daily & Nece 1960), $\rho = 1.225$ kg/m³, $R = 0.15$ m. Note: $(0.15)^5$ evaluates to 7.59×10^{-5} m^5. Substituting all values ($\omega = 20$ rad/s):

$$Q_{drag} = 0.5 \times 1.225 \times 0.04 \times 400 \times (7.59 \times 10^{-5}) \approx 7.4 \times 10^{-4}\ \text{N·m}$$

This is a negligible drag torque compared to the useful cylinder torque of ~10 N·m. Aerodynamic drag therefore contributes under 3% of total losses; spring hysteresis (metal flexing) dominates the 25% loss category.

• Structural/metal flexing losses: Estimated at 2–3% based on spring hysteresis data for SAE 9254 spring steel (energy loss per loading cycle ≈ 2% per Wahl spring design methodology in Shigley and Mischke).

8.2 Energy Distribution with Uncertainty Bounds

Energy Channel	Estimated %	Uncertainty Range	Estimation Basis
Useful Rotational Output	40%	±8%	By subtraction from total losses
Bearing Friction Heat Loss	35%	±4%	SKF friction torque model, μ = 0.001–0.0015
Aerodynamic & Flexing Loss	25%	±6%	Drag formula + spring hysteresis model
Total	**100%**	—	Conservation of energy (1st Law)

Table 3. Analytical energy distribution estimates with uncertainty bounds and estimation basis. All values require experimental validation.

8.3 Comparison with Published Experimental Data

Study	System Type	Useful Output Efficiency	Method

Parashar et al. (2025)	Spring-powered generator, single cylinder	25–40% (measured)	Instrumented prototype
This study (2026)	Spring-powered V8, 8-cylinder, staggered crankshaft	40% ±8% (estimated)	Analytical model, no prototype

Table 4. Comparison of efficiency estimates with the most closely related published experimental study. The analytical estimate of 40% falls within the published experimental range of 25–40%, providing partial indirect support for the model, but does not substitute for direct measurement.

The alignment between the analytical estimate (40%) and Parashar et al.'s upper experimental bound (40%) is notable but should be interpreted cautiously. The two systems differ in cylinder count, crankshaft geometry, and flywheel configuration. The multi-cylinder V8 arrangement introduces additional bearing contact points compared to a single-cylinder design, which would tend to increase friction losses. It is therefore possible that the true useful output efficiency of the V8 configuration is somewhat lower than 40% — potentially closer to the 25–35% range — once all eight bearing assemblies are accounted for. This is a key question for experimental investigation.

8.4 First and Second Laws of Thermodynamics

The First Law (conservation of energy, $\Delta U = Q - W$) is fully satisfied: total elastic PE input equals the sum of useful mechanical output plus all dissipative losses. No energy is created within the system.

The Second Law ($\Delta S \geq 0$) is also fully satisfied. The 60% of input energy dissipated as heat and mechanical losses represents an irreversible entropy increase in the environment. This dissipation cannot be recovered and fed back into the springs. Runtime is strictly finite and bounded by initial spring loading energy. These two laws categorically rule out perpetual motion.

8.5 Refutation of Perpetual Motion Claims

Spring-powered mechanical devices frequently attract perpetual motion claims, particularly when a flywheel maintains rotation after apparent spring discharge. This paper refutes such claims on three specific grounds:

- Energy source identification: All operational energy originates from human muscular work during spring loading. The machine is an energy converter, not an energy source. The human is the engine.
- Finite runtime: The machine invariably stops when all spring energy is exhausted ($\Delta PE = 0$). Extended runtime after spring discharge is attributable exclusively to flywheel momentum — itself derived from the original spring loading energy, not from any new energy source.
- Measurable losses: The analytically estimated 60% energy loss to friction and aerodynamic drag confirms irreversible thermodynamic dissipation, consistent with the Second Law and categorically inconsistent with any perpetual motion claim.

9. Runtime Prediction, Spring Fatigue, and Safety

9.1 Runtime Prediction Formula

The operational runtime t_{run} of the machine — from full spring release to complete stop — can be estimated from first principles. After all springs discharge, the flywheel's kinetic energy $E_k = \frac{1}{2}I\omega^2$ is dissipated solely by bearing friction. The deceleration torque due to bearing friction is $\tau_f = M_{friction} \times$

N_bearings, where N_bearings is the number of active bearing contact points. The angular deceleration is $\alpha = \tau_f / I$. Assuming constant friction torque (which is a simplification — in reality it varies with speed), the coast-down time from initial angular velocity ω_0 to rest is:

$$t_{coast} = \omega_0 \cdot I / \tau_f$$

For the specified flywheel ($I = 0.251$ kg·m²), $\omega_0 = 20$ rad/s, and estimated total bearing friction torque $\tau_f \approx 0.15$ N·m (from 10 bearing assemblies at $\mu = 0.001$, mean load 300 N, bore 25 mm):

$$t_{coast} = 20 \times 0.251 / 0.15 \approx 33.5 \text{ seconds}$$

Total operational runtime including the spring-driven phase depends on how quickly the springs discharge. If all eight springs discharge over approximately one full revolution ($\Delta\theta = 2\pi$ rad) at mean $\omega = 20$ rad/s, the spring-driven phase lasts ≈0.31 seconds, after which the machine coasts for ≈34 seconds on flywheel momentum alone. These values are analytical estimates and will vary significantly with actual spring stiffness, loading displacement, and bearing condition.

> **Note:** The runtime formula above assumes constant friction torque and ignores speed-dependent aerodynamic drag. A more accurate model would use a nonlinear ODE: $I(d\omega/dt) = -\tau_f - k_{drag}\omega^2$, solved numerically. This is recommended for future analytical refinement.

9.2 Spring Fatigue Life Analysis

Spring fatigue is a genuine engineering concern that affects long-term reliability of the machine. Repeated loading and unloading of the springs induces cyclic torsional stress in the coil wire, which — above the fatigue endurance limit — leads to progressive crack initiation and eventual fracture. Using Wahl's correction factor (K_w) for curved beam stress in coil springs (as presented in Shigley and Mischke), the maximum shear stress in the coil wire is:

$$\tau_{max} = K_w \cdot (8FD / \pi d^3)$$

where F is the spring load, D is the mean coil diameter, d is the wire diameter, and $K_w = (4C-1)/(4C-4) + 0.615/C$ with spring index $C = D/d$. For the design parameters ($D = 70$ mm, estimated wire $d = 6$ mm, $C \approx 11.7$, $F = 250$ N): $K_w \approx 1.12$, $\tau_{max} \approx 1.12 \times (8 \times 250 \times 0.07) / (\pi \times 0.000216) \approx 232$ MPa. For SAE 9254 spring steel, the corrected endurance limit in torsion is approximately $S_{se} \approx 310$–380 MPa (per Shigley and Mischke, Table 10-6). The stress ratio $\tau_{max}/S_{se} \approx 0.65$–$0.75$ gives a conservative fatigue life estimate exceeding 100,000 full load cycles — sufficient for extended educational use.

However, fatigue life is highly sensitive to surface finish, corrosion, and over-compression beyond the design displacement x. The machine should never be loaded beyond the design compression of 50 mm per spring. Springs showing visible surface corrosion, permanent set (failure to return to natural length), or cracking should be replaced immediately.

9.3 Safety Considerations

Compressed spring systems store significant elastic potential energy that can release suddenly and violently if containment fails. This section identifies the primary hazard scenarios and recommended mitigations for the spring-powered V8 engine model.

- Spring ejection hazard: If a spring anchor weld fails or a piston rod shears, the compressed spring can propel the rod at high velocity. Mitigation: design all spring anchor welds to a safety factor of ≥4 against the maximum spring pre-load force; install a perforated metal safety shield around the spring assemblies during operation.

• Detent pin failure: Failure of a detent pin during manual loading can cause uncontrolled spring release toward the operator. Mitigation: use hardened steel detent pins rated to ≥2× maximum spring load; never place hands in the spring travel path during loading.

• Flywheel fragmentation: If the flywheel develops a fatigue crack and fractures at operating speed, fragments are ejected at high velocity. Mitigation: perform visual inspection of the flywheel before each use; do not exceed the design operating speed; consider installing a partial flywheel guard.

• Over-compression: Loading springs beyond their design displacement increases wire stress above the fatigue endurance limit and risks coil binding or permanent set. Mitigation: mark the maximum safe loading position on each piston rod with a physical stop collar.

10. Recommended Experimental Validation Protocol

As stated throughout this paper, all energy distribution figures are analytical estimates. The single highest-impact improvement would be constructing a physical prototype and collecting even basic measurements. The following protocol describes minimum viable experimental validation using readily available equipment.

Measurement	Equipment	Parameter Validated	Target Accuracy
Spring force vs. displacement	Hanging scale or force gauge	Spring constant k; confirm k = 5,000 N/m	±5%
Crankshaft RPM during operation	Smartphone tachometer app (reflective tape method)	Operating ω; validate flywheel sizing model	±2 RPM
Coast-down time after spring discharge	Stopwatch; smartphone slow-motion video	Validate runtime prediction formula (Section 9.1)	±0.5 s
Bearing temperature rise after operation	Infrared thermometer (< £20)	Bearing friction heat loss; validate 35% estimate	±1°C
Total runtime per full loading cycle	Stopwatch	Overall energy budget; cross-check all estimates	±0.5 s

Table 5. Minimum viable experimental validation protocol. All listed measurements can be performed with low-cost consumer equipment.

Collection of even these five basic measurements would transform this paper from a theoretical design study into an experimental research paper — a categorically different level of scientific credibility. The spring force measurement and RPM reading in particular require no specialized equipment and could be completed in under one hour with a constructed prototype.

11. Discussion

11.1 Engineering and Educational Significance

The spring-powered V8 engine model represents a pedagogically valuable physical embodiment of multi-domain mechanical engineering principles. Unlike simulation software or static diagrams, a physical prototype makes abstract principles — energy conversion efficiency, bearing losses, flywheel

dynamics, crankshaft kinematics — directly observable and measurable. This positions the machine as an effective STEM teaching tool that makes all five fundamental physics domains (mechanics, thermodynamics, tribology, dynamics, materials) simultaneously visible.

11.2 Limitations of This Study

Three key limitations are acknowledged. First and most importantly, no physical prototype was constructed or tested for this study — all quantitative figures are analytical estimates. Second, the energy distribution model assumes steady-state operation, whereas in reality the spring force declines during discharge, producing transient behavior that the steady-state model does not capture. Third, the flywheel moment of inertia calculation assumes a perfectly uniform solid disc — any deviation from this geometry requires recalculation.

11.3 Future Research Directions

Priority future work includes: (1) constructing and instrumenting a physical prototype to validate the energy distribution model; (2) parametric experimental testing of spring constants in the range k = 2,000–8,000 N/m to map efficiency vs. spring stiffness; (3) high-speed video analysis of crankshaft motion during spring discharge to characterize actual angular velocity variation; and (4) long-duration fatigue testing of the spring assemblies to empirically characterize failure cycles under repeated loading.

12. Conclusion

This paper has presented a theoretical mechanical design and analytical study of a hand-loaded spring-powered V8 engine model, with full transparency about the study's theoretical nature and the analytical basis of all quantitative estimates. The design demonstrates a complete energy conversion pathway from manually stored elastic potential energy to smooth rotational mechanical output, governed throughout by Hooke's Law, Newtonian mechanics, and the Laws of Thermodynamics.

The crankshaft's eight-pin 90° cross-plane configuration provides evenly-phased torque delivery. The specified solid disc flywheel ($I = 0.251$ kg·m²) provides substantial momentum smoothing, with a derived coast-down time of approximately 34 seconds after spring discharge. However, the flywheel is marginally undersized relative to the 5% speed-fluctuation target ($I_{required} = 0.3125$ kg·m²): either the flywheel mass should be increased to ~28 kg or the fluctuation tolerance relaxed to ~6.3% — a concrete design revision recommended for prototype construction. Analytical energy estimates suggest ≈40% useful output efficiency with ±8% uncertainty — consistent with the published experimental range of 25–40% from the most closely related prior study, though direct experimental comparison is not yet possible.

Spring fatigue analysis indicates a theoretical life exceeding 100,000 cycles under design conditions. Safety hazards specific to compressed spring systems are identified and mitigations specified. A minimum viable experimental validation protocol is provided that requires only consumer-grade equipment. The construction of a physical prototype and collection of even basic measurements is identified as the single highest-impact next step for this research.

Acknowledgments

The author acknowledges the use of AI-assisted tools for literature survey, figure generation, and manuscript preparation support. All engineering analyses, design decisions, interpretations, and

conclusions are solely those of the author.

References

[1] Parashar, N., Saini, B., Sharma, H., Yadav, H., Pooniya, K., & Modi, B. (2025). "Spring Mechanism Runs Forever: DIY Free Energy Generator." International Journal of Research and Analytical Studies in Engineering Technology (IJRASET). doi:10.22214/ijraset.2025.70689. [Title reflects authors' framing; paper content rigorously debunks perpetual motion claims through thermodynamic analysis.]

[2] Achten, P. A. J. (1994). "A Review of Free Piston Engine Concepts." SAE Technical Paper Series 941776. Society of Automotive Engineers. doi:10.4271/941776.

[3] Robinson, M. C., & Clark, N. N. (2014). "Spring-Varied Free Piston Linear Engine Devices." ASME 2014 Internal Combustion Engine Division Fall Technical Conference. ICEF2014-5628. doi:10.1115/ICEF2014-5628.

[4] Mikalsen, R., & Roskilly, A. P. (2007). "A Review of Free-Piston Engine History and Applications." Applied Thermal Engineering, 27(14–15), 2339–2352. doi:10.1016/j.applthermaleng.2007.03.015.

[5] Fredriksen, T. O. (2020). "Modeling and Experimental Validation of a Spring-Dominant Free Piston Engine Generator." M.Sc. Thesis, West Virginia University. Morgantown, WV, USA.

[6] Shigley, J. E., & Mischke, C. R. (2011). Mechanical Engineering Design. 9th ed. McGraw-Hill. ISBN: 978-0-073-52928-8. [Sections 10-4 to 10-7: Spring design and fatigue; Section 16-4: Flywheel sizing].

[7] Meriam, J. L., & Kraige, L. G. (2012). Engineering Mechanics: Dynamics. 7th ed. John Wiley & Sons. ISBN: 978-1-118-08361-5. [Chapter 6: Planar kinetics of a rigid body — used in crankshaft torque analysis].

[8] SKF Group. (2018). SKF Rolling Bearings Catalogue. Publication 10000/2 EN. SKF Group, Gothenburg, Sweden. [Bearing friction torque model applied in Section 8.1 loss estimation].

[9] Cengel, Y. A., & Boles, M. A. (2014). Thermodynamics: An Engineering Approach. 8th ed. McGraw-Hill Education. ISBN: 978-0-073-38817-7. [First and Second Law formulations used in Section 8.4].